Applied Surface Science 258 (2012) 3051–3057

Contents lists available at SciVerse ScienceDirect

Applied Surface Science

journal homepage: www.elsevier.com/locate/apsusc

Effects of duty cycle on microstructure and corrosion behavior of TiC coatings prepared by DC pulsed plasma CVD

Ali Shanaghi[a,b,1], Ali Reza Sabour Rouhaghdam[a,*], Shahrokh Ahangarani[c], Paul K. Chu[b], Taghi Shahrabi Farahani[a]

[a] Surface Engineering Laboratory, Materials Engineering Department, Faculty of Engineering, Tarbiat Modares University, P.O. Box 14115-143, Tehran, Iran
[b] Department of Physics & Materials Science, City University of Hong Kong, Tat Chee Avenue, Kowloon, Hong Kong, China
[c] Advanced Materials & Renewable Energies Department, Iranian Research organization for science and technology, P.O. Box 15815-3538, Tehran, Iran

ARTICLE INFO

Article history:
Received 26 June 2011
Received in revised form 29 October 2011
Accepted 8 November 2011
Available online 18 November 2011

Keywords:
TiC nanostructure coating
Corrosion behavior
Plasma CVD
Duty cycle

ABSTRACT

Titanium carbide coatings are deposited on hot-work steel (H_{11}) by plasma-assisted chemical vapor deposition (PACVD) and the dependence of the corrosion behavior on fabrication parameters is investigated. Grazing incidence X-ray diffraction (GIXRD), field emission scanning electron microscopy (FESEM), Raman and electrochemical tests are used to study the structure as well as corrosion behaviors. Grazing incidence X-ray diffraction reveals the (2 0 0) plane implying that the TiC coatings are deposited *via* the kinetics-limited crystal growth mechanism and under thermodynamically stable conditions. The SEM results indicate that the formation of a homogeneous and uniform titanium carbide nanostructure coatings. Potentiodynamic and electrochemical impedance tests performed in 0.5 M H_2SO_4 and 0.05 M NaCl show that the TiC coating produced using a 40% duty cycle possesses high corrosion resistance in both media. The R_p values of the TiC coating (50% duty cycle) in 0.05 M NaCl and the other TiC coating (40% duty cycle) in 0.5 M H_2SO_4 are approximately four and sixteen orders of magnitude higher than that of the bare steel, respectively. Our results reveal that the duty cycles not only affect the structure and morphology of the coatings but also influence the electrochemical properties.

1. Introduction

Titanium carbide (TiC) coatings have many industrial applications because of its high hardness, low friction coefficient, as well as excellent wear resistance and corrosion resistance [1]. A number of methods such as physical vapor deposition (PVD), pulsed laser deposition (PLD), and chemical vapor deposition (CVD) have been used to deposit the hard coatings and the properties of TiC are known to depend on the deposition techniques and conditions [2–4]. Contrary to conventional CVD processes in which high-quality coatings are typically deposited at a high temperature (500–1050 °C), plasma-assisted chemical vapor deposition (PACVD) allows the fabrication of wear and corrosion resistant coatings on temperature-sensitive materials [5,6]. In fact, plasma CVD has been employed to deposit TiC coatings at a relatively low temperature [7]. Further studies indicate that the properties of titanium carbide are related to the chemical composition and texture and also affect the adhesion and residual stress in the thin film [3–10].

It is still challenging to deposit TiC coatings on metals because the materials are metastable and the PACVD reactions are quite complicated. Several fabrication parameters such as temperature, gas ratio, and duty cycle can affect the properties of TiC coatings. In addition, despite the widespread use of titanium carbide in hard coatings, the dependence of the corrosion behavior of the materials on some fabrication parameters is not well understood. Among the various parameters, which affect the properties of TiC nanostructured coatings, the duty cycle plays an essential role as a thermodynamic and kinetic parameter. It has been shown that the duty cycle and pulse frequency affect the plasma density in the plasmas and the processing rate can be improved. Furthermore, it has been demonstrated quantitatively that the ionization process is altered by a pulsed plasma process [12–14]. The objective of the present work is to investigate the corrosion mechanism of TiC coatings deposited by PACVD on hot-work tool steel (AISI H11 – DIN 1.2343) in aggressive media such as NaCl and H_2SO_4 solutions and to study the influence of the duty cycle on structure, morphology, chemical composition, and corrosion behavior of TiC.

* Corresponding author.
E-mail addresses: alishanaghi@gmail.com, shanaghi@modares.ac.ir, Shanagali2@student.cityu.edu.hk (A. Shanaghi), sabour01@modares.ac.ir (A.R.S. Rouhaghdam), sh.ahangarani@gmail.com (S. Ahangarani), paul.chu@cityu.edu.hk (P.K. Chu), tshahrabi34@modares.ac.ir (T.S. Farahani).
[1] Tel.: +98 9188644460 (Iran)/+852 34425484 (Hong Kong, China); fax: +98 2188332900.

0169-4332/$ – see front matter © 2011 Elsevier B.V. All rights reserved.
doi:10.1016/j.apsusc.2011.11.036

Table 1
treatments parameters for deposition of the TiC coatings.

Parameters	Values
Pulsed voltage (V)	590
Pressure (mbar)	4–8
Duty cycles (%)	33, 40 and 50
Processing time (h)	2
H_2 (nl/min)	1.6
Ar (nl/min)	0.05
CH_4 (nl/min)	0.1–0.5
$TiCl_4$ (nl/min)	0.05
Temperature (°C)	490

2. Material and methods

The TiC coatings were deposited in a PACVD reactor using a $TiCl_4$–CH_4– H_2–Ar gas mixture. The plasma was triggered by a DC pulse power supply and the pressure in the reaction chamber was 5 mbar. Table 1 lists the important instrumental conditions.

The hot-working die steel grade AISI H_{11} (DIN 1.2343) was used as the substrate and Table 2 shows the composition of the materials determined by spark emission spectroscopy.

The substrate temperature was controlled by an auxiliary heating system in addition to the intrinsic sputtering effect. Three different duty cycles were selected to investigate the influence on the corrosion behavior of the coatings.

Table 2
Chemical composition of the AISI H_{11} determined by spark emission spectroscopy.

Composition	C	Si	V	Cr	Mo	Mn	P
Weight percent	0.36	0.56	0.4	4.6	0.52	0.37	0.01

The crystalline structure of the coating was determined by grazing incidence X-ray diffraction (GIXRD) (Philips PW-1730 diffractometer) in the continuous scanning mode and using Cu K_α radiation ($\lambda = 0.154056$ nm). The tube voltage was 40 kV, current was 30 mA, 2θ was 10–80°, step was 0.05°, and sweep rate was 0.05°/s. The full-width at half-maximum (FWHM) of the Bragg peaks is used to approximate grain size base on the Scherrer formula [8]:

$$D = \frac{0.9\lambda}{\beta \cos\theta}, \quad (1)$$

where D is grain size, β is the FWHM of the Bragg peak, and θ is the Bragg reflection angle. The structure was also analyzed by Raman spectroscopy (Almega Thermo Nicolet Dispersive Raman Spectrometer) in the spectral range of 100–1800 cm^{-1}. The surface morphology and roughness of the coatings were measured by scanning electron microscopy (SEM) (Philips XL-30). The electrochemical measurements were performed using the EG&G potentiostat/galvanostat (Prinston, model 273A) in 0.5 M H_2SO_4

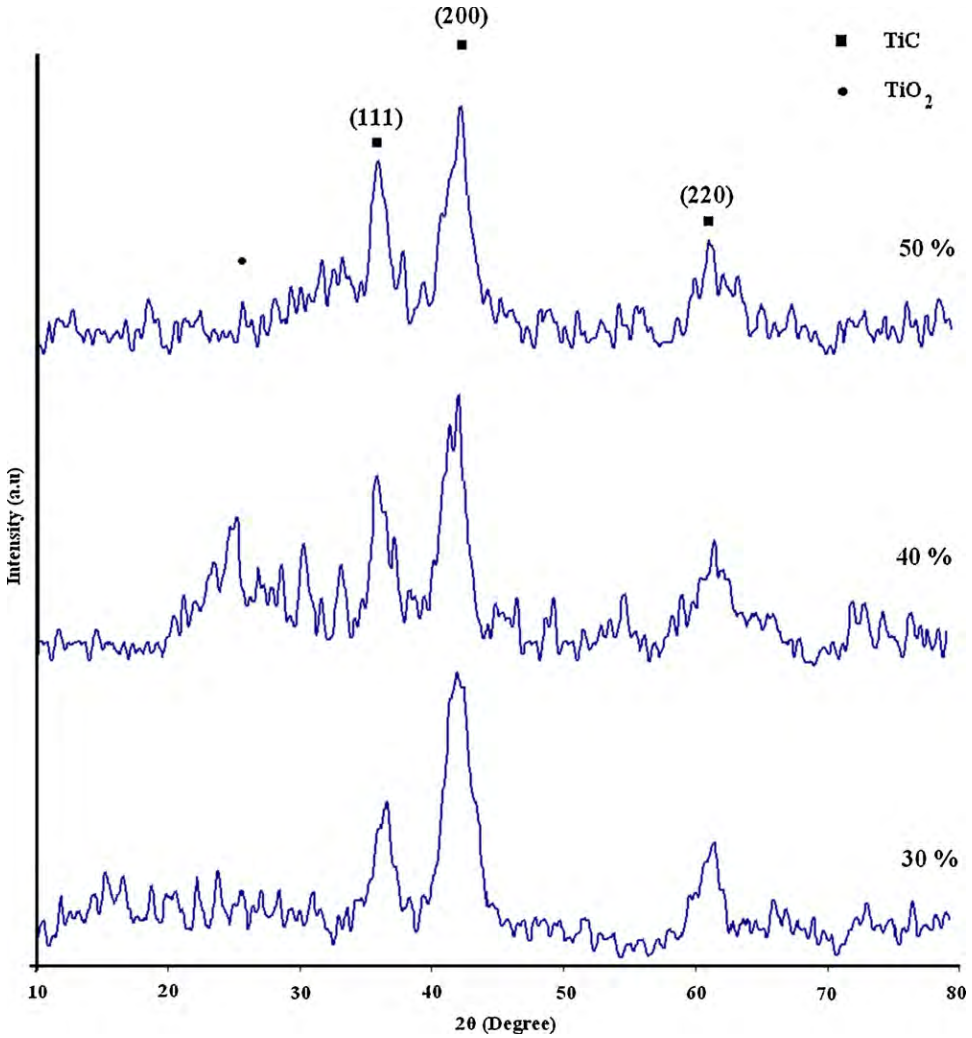

Fig. 1. GIXRD diffraction patterns acquired from the TiC_X coatings using the three duty cycles of 33%, 40%, and 50%.

and 0.05 M NaCl solutions. The standard electrochemical cell consisted of three electrodes including the coated sample as the working electrode, saturated calomel as the reference electrode, and platinum net as the auxiliary electrode. The EIS experiments were carried out at a frequency range of 10 mHz to 100 kHz at the open circuit potential and the perturbation amplitude was 10 mV. Each test was repeated three times to improve the statistics.

3. Results and discussion

Fig. 1 depicts the GIXRD patterns of the coatings deposited at 490 °C using the three duty cycles of 33%, 40%, and 50%. The reference peaks of TiC are in accordance with the ICCC-JCPDS value (titanium carbide No. 31-1400). The (2 0 0) plane is revealed to be the preferred structure, implying that the TiC coating is deposited *via* kinetics-limited crystal growth [9] and under thermodynamically stable conditions because the lowest energy surface in the TiC crystal is the (2 0 0) plane [10,11]. The GIXRD pattern also indicates an exclusively face-center-cubic (fcc) structure. Fig. 1 shows that by increasing the duty cycle from 33% to 40%, the TiO_2 phase emerges and vanishes if the duty cycle is raised further from 40% to 50%. An oxide impurity is observed based on the broad peak of (2 2 0) from the 40% duty cycle sample. The (2 2 0) plane is not thermodynamically stable relative to the (2 0 0) and (1 1 1) planes and the broad peak of the (2 2 0) plane indicates that the grain size decreases. Hence, the specific surface of TiC increases and finally the titanium oxide layer is formed upon exposure to air.

Fig. 2 displays the SEM images of the three TiC coatings deposited using duty cycles of 33%, 40%, and 50% as well as the cross sections showing the coating thickness. An island-like morphology is observed due to axial growth of TiC during PACVD. The surface morphology of the two coatings produced at duty cycles of 33% and 50% is about the same, that is, similar microstructure (rough surface) containing 0.1–0.2 μm aggregates of 4–10 nm TiC grains. However, as the duty cycle is raised, the surface becomes smoother and denser. The surface morphology plays an important role in the corrosion behavior. According to the Scherrer formula, the grain size of the TiC coatings is 15, 7, and 5 nm for duty cycles of 33%, 40%, and 50% (Fig. 1). The fine-grained morphology is confirmed by the smooth surface and relatively small thickness (3 μm) of the TiC coating shown in Fig. 2.

Raman scattering is a powerful and non-destructive technique to study the microstructure of coatings [12]. The Raman spectra in the range of 100–1800 cm^{-1} of the TiC samples are shown in Fig. 3. Scattering in the acoustic range is mainly determined by the vibrations of the heavy Ti ions (typically 150–350 cm^{-1}) and in the optical range by the vibrations of the lighter C ions (typically 550–1300 cm^{-1}). The peaks at 230, 289 and 588 cm^{-1} arise from first order transverse acoustic (TA) and transverse optical (TO) modes of TiC, respectively. Owing to the oxide layer on the surface, additional peaks at 152 and 428 cm^{-1} characteristic of TiO_2 [13] are observed. It is also known that a surface titanium oxide layer is formed upon exposure to air [14]. However, the amounts of the oxide impurities observed from the 33% and 50% duty cycle samples are relatively low (1–3 vol.%) and cannot be detected by conventional X-ray diffraction techniques.

Figs. 4 and 5 present the potentiodynamic results obtained from the bare steel substrate and TiC coatings in 0.05 M NaCl and 0.5 M H_2SO_4 solutions at room temperature (28 °C). The data are analyzed to obtain the different electrochemical parameters and the results are shown in Table 3. The open circuit potentials of the uncoated steel in 0.05 NaCl and 0.5 H_2SO_4 solutions are −602 mV and −609 mV versus SCE, respectively.

The TiC coatings change the open circuit potentials from negative to positive and the electrochemical properties also depend

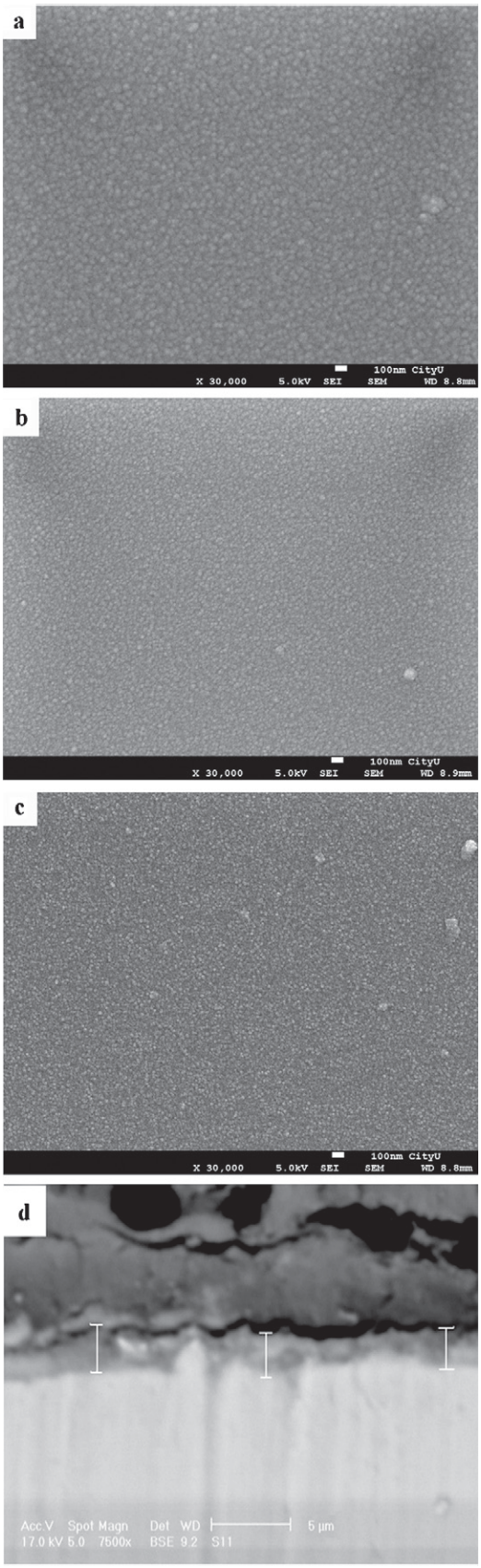

Fig. 2. SEM micrographs of the TiC coatings deposited using three duty cycles: (a) 33%, (b) 40%, and (c) 50% and (d) shows the cross-section of the coating.

Table 3
Polarization parameters of the uncoated steel and TiC coatings in 0.05 M NaCl and 0.5 M H_2SO_4 solutions.

Solution	Duty cycle (%)	β_a (mV/dec)	β_c (mV/dec)	E_{corr} (mV)	i_{corr} (μA/cm^{-2})	R_p (Ω/cm^{-2})
0.05 M NaCl						
Bare steel		114	147	−602	63	443
	33	128	162	−533	0.81	38,380
TiC coating	40	168	210	−441	0.024	684,380
	50	146	185	−550	0.17	208,699
0.5 M H_2SO_4						
Bare steel		54	91	−609	1012	15
	33	71	102	−542	106	172
TiC coating	40	95	103	−477	13	1652
	50	87	99	−562	68	296

on the duty cycles. The data indicate that corrosion resistance is improved and substrate corrosion is removed therewith. Both the anodic and cathodic branches shift towards lower currents, i.e. lower rates of the metal corrosion. Based on the linear polarization data, the polarization resistance of the bare steel and TiC coatings can be derived using the following formula:

$$R_p = \frac{\beta_a \times \beta_c}{2.3 \times i_{corr}(\beta_a + \beta_c)}, \quad (2)$$

where β_a, β_c, E_{corr}, i_{corr}, and R_p are the Tafel slopes parameters of the anodic and cathodic reactions, open circuit potential, corrosion current density, and polarization resistance, respectively [15].

The polarization resistance, R_p is an important kinetics parameter. A larger R_p indicates a lower rate for the metal corrosion reaction. Table 3 shows that with increasing duty cycles from 33% to 50%, the polarization resistance of the TiC coatings in 0.05 M NaCl and 0.5 M H_2SO_4 increases by about 17 and 9 times, respectively. More specifically, the corrosion resistance of the TiC is enhanced when the duty cycle is increased from 33% to 40% but decreases from 40% to 50%. The trend in the corrosion resistance can be explained by the formation of defects and pores in the coating. Figs. 6 and 7 depict the SEM micrographs of the bare steel and 3 TiC coatings after potentiodynamic tests in 0.05 M NaCl and 0.5 M H_2SO_4 solutions, respectively. According to Figs. 6a and c and 7a, b and d, the bare steel and TiC coatings exhibit pitting and uniform corrosion in both solutions, but Figs. 6b and d and 7c indicate grain boundary corrosion. Actually, the TiC coating produced using at a 33% duty cycle shows many open pores (related to the island-like morphology and distance between them) and there are many corrosion pits after immersion in the aggressive solution. It has worse corrosion resistance due to the less dense structure and size of

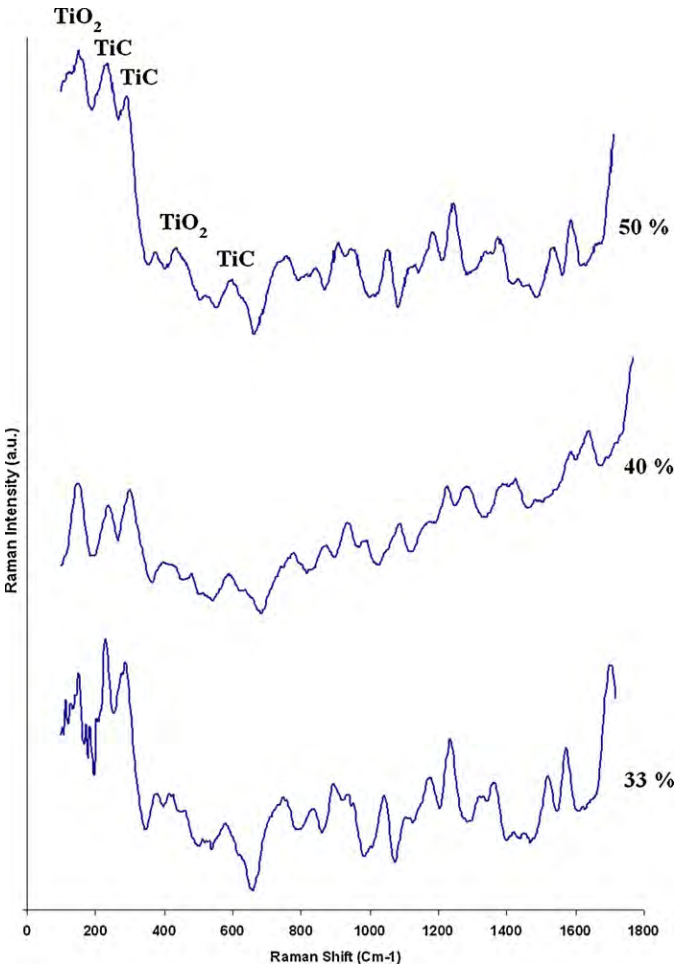

Fig. 3. Raman spectra of the TiC coatings prepared using duty cycles of 33%, 40%, and 50%.

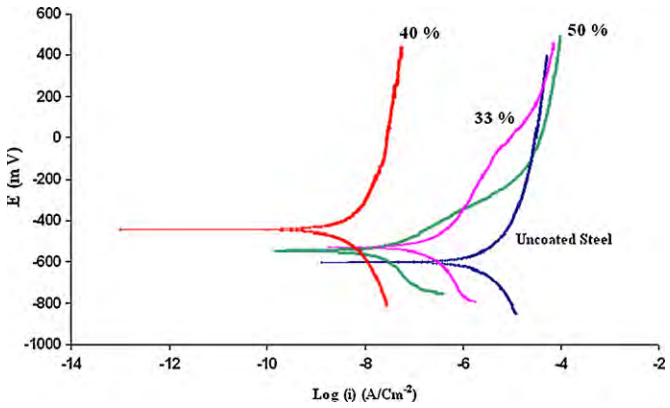

Fig. 4. Potentiodynamic results obtained from the uncoated steel and TiC coatings produced using duty cycles of 33%, 40%, and 50% in 0.05 M NaCl.

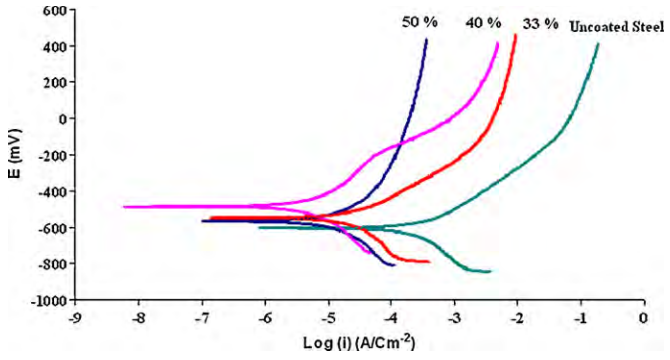

Fig. 5. Potentiodynamic results obtained from the uncoated steel and TiC coatings produced using duty cycles of 33%, 40%, and 50% in 0. 5 M H_2SO_4.

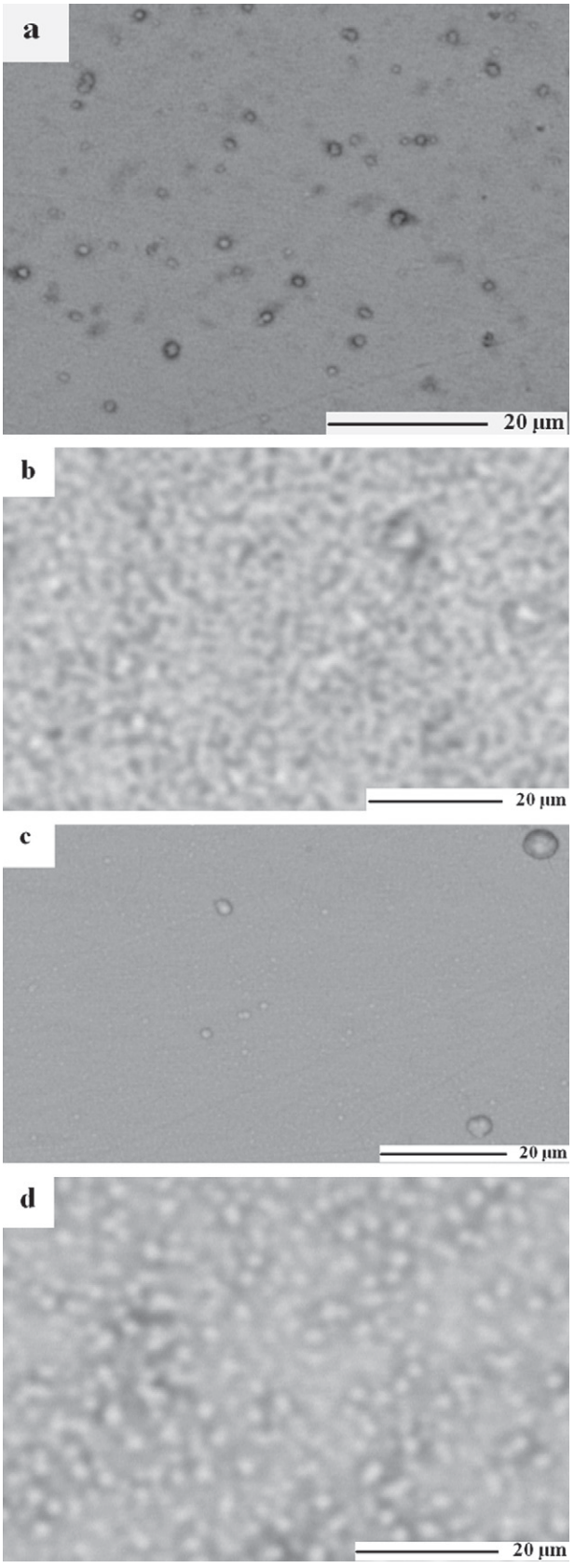

Fig. 6. SEM micrographs: (a) bare steel, (b) TiC coating produced at a duty cycle of 33%, (c) TiC coating produced at a duty cycle of 40%, and (d) TiC coating produced at a duty cycle of 50% in 0.05 M NaCl.

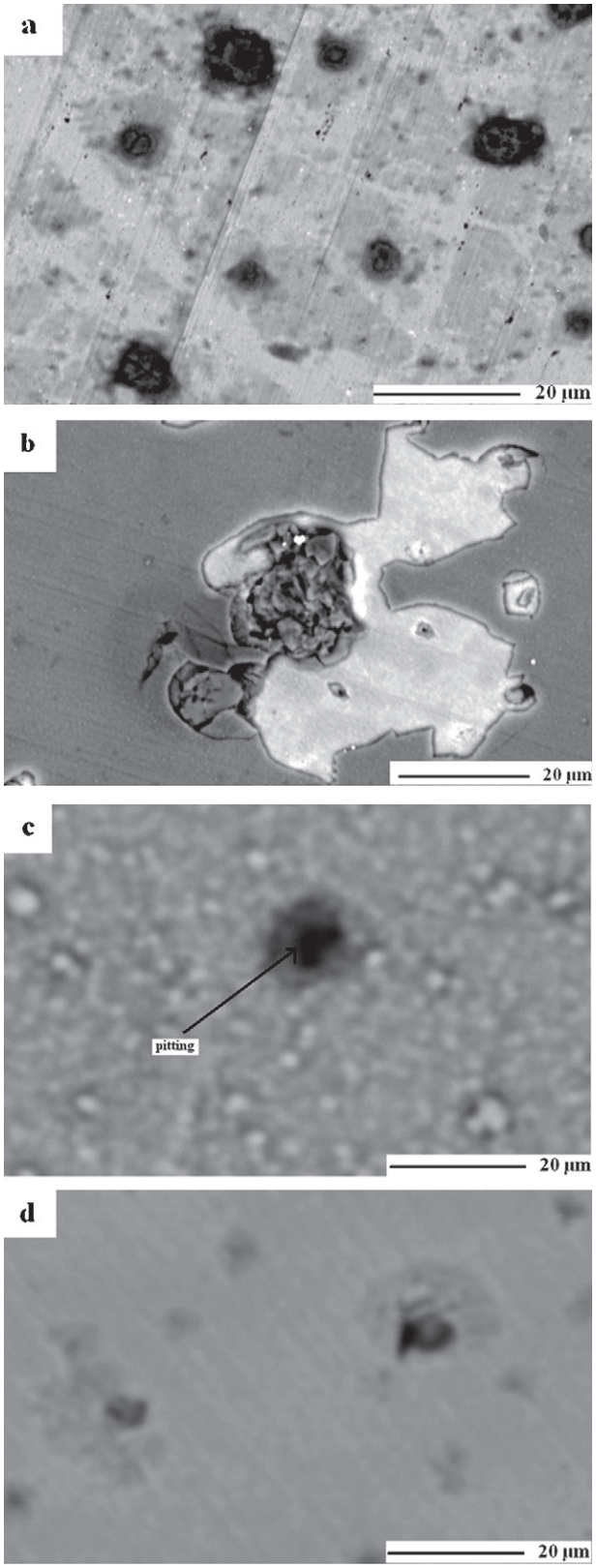

Fig. 7. SEM micrographs: (a) bare steel, (b) TiC coating produced at a duty cycle of 33%, (c) TiC coating produced at a duty cycle of 40%, and (d) TiC coating produced at a duty cycle of 50% in 0.5 M H_2SO_4.

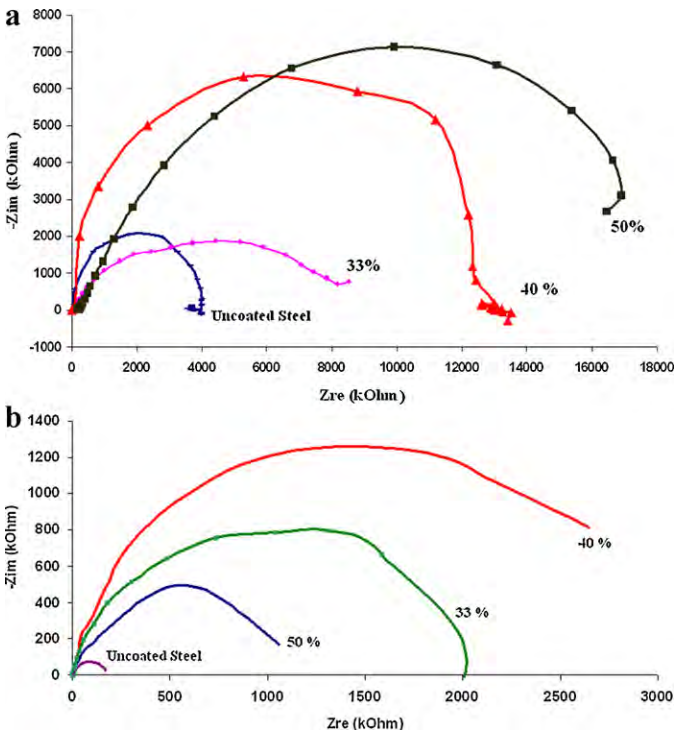

Fig. 8. Nyquist plots of the bare steel and 3 TiC coatings: (a) 0.05 M NaCl and (b) 0.5 M H_2SO_4 solutions.

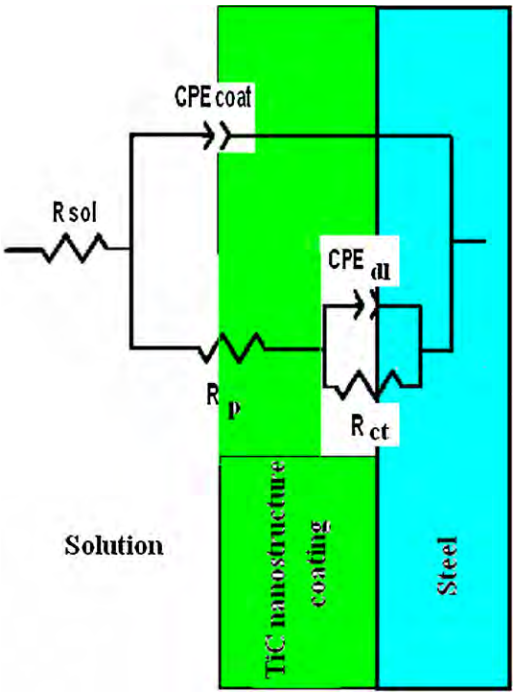

Fig. 9. Equivalent electrical model.

corrosion pits being greater than those observed from the 50% to 40% duty cycle samples. The corrosion mechanism may be explained as follows. Initially, general corrosion occurs at the open pores, grain boundary, and defects of the coating. As time elapses, grain boundary corrosion causes the islands of agglomerated TiC to separate and corrosion of the islands occur rapidly. Finally, the islands of agglomerated TiC disappear and a pit is formed. The corrosion reaction can be inferred by observing the breakdown of the TiC film.

It has been suggested that the presence of a small amount of the TiO_2 phase, especially in the 40% duty cycle sample, may improve the stability of the TiC coatings and decrease the amount of defect and thermodynamically unstable phases in contact with the aggressive solution finally improving the pitting resistance of the TiC coatings.

According to Fig. 7c, the TiC coating undergoes both pitting and grain boundary corrosion in 0.5 M H_2SO_4 rather than in 0.05 M NaCl. It is clear that the corrosion damage on the bare steel and TiC coatings in 0.5 M H_2SO_4 is more than that in 0.05 M NaCl. The corrosion mechanism of the TiC coatings prepared at duty cycles of 33% and 50% in both solutions appears to be similar and it is consistent with the morphology of the TiC coatings.

Electrochemical impedance spectroscopy (EIS) provides important information about the corrosion behavior of the TiC coatings in aggressive media such as 0.05 M NaCl and 0.5 M H_2SO_4 used in our experiments. Fig. 8 shows the Nyquist impedance of the bare steel and TiC coatings, revealing that R_p of the TiC coatings varies with the processing parameters in the following order: R_p (33%) > R_p (40%) > R_p (50%) and R_p (33%) > R_p (50%) > R_p (40%) in 0.05 M NaCl and 0.5 M H_2SO_4, respectively. In 0.05 M NaCl, the impedance spectra of the bare steel and TiC coatings produced at duty cycles of 40% and 50% consist of a large capacitive loop at high frequencies followed by a small inductive loop at low frequencies, whereas the impedance spectra of the coatings prepared at a duty cycle of 33% exhibits exhibit one single depressed semicircle. In contrast, the impedance spectra obtained from the bare steel and TiC coatings in 0.5 M H_2SO_4 is quite different. A large capacitive loop at high frequencies followed by a small inductive loop at low frequencies is usually related to the charge transfer of the corrosion process and double layer behavior. On the other hand, the low frequency inductive loop is typically attributed to the relaxation process [16]. As shown in Fig. 8a and b, the impedance data suggest good corrosion resistance in 0.05 M NaCl, but rapid deterioration occurs in 0.5 M H_2SO_4 due to pores in the TiC coatings as shown in Figs. 6 and 7. Hence, a pitting mechanism takes place and dissolution of the corrosion products increases the acidity in the vicinity of the pits, especially in 0.5 M H_2SO_4. These capacitive loops in both solutions are not perfect semicircles attributable to the frequency dispersion effect as a result of the roughness and inhomogeneous structure of the coatings [17].

Fig. 9 shows the equivalent circuit based on the EIS data. This circuit is commonly utilized to simulate coating/substrate systems [18–21]. The different elements are described as follows. R_s is the resistance of the electrolyte between the working and reference electrode and R_p corresponds to the polarization resistance at the coating/electrolyte interface in the micropores. CPE_{coat} and CPE_{dl} are the capacitances represented by the constant-phase elements (CPE). Generally, a CPE is used instead of pure capacitance because of the relaxation time induced by the inhomogeneities on the microscopic level at the electrode/electrolyte interface [22]. CPE_{coat} represents the capacitance of the TiC nanostructure coatings whereas CPE_{dl} is the capacitance at the substrate/electrolyte interface. R_{ct} is the charge transfer resistance at the substrate/coating interface.

Table 4 summarizes the fitted resistance and capacitance values of the 3 TiC coatings in 0.05 M NaCl and 0.5 M H_2SO_4. The R_p values of the TiC coating (50% duty cycle) in 0.05 M NaCl and the other TiC coating (40% duty cycle) in 0.5 M H_2SO_4 are approximately four and sixteen orders of magnitude higher than that of the bare steel, respectively, indicating that the TiC coatings inhibit charge transfer at the coating/electrolyte interface consequently enhance the corrosion resistance effectively. These results confirm that high corrosion resistance can be obtained by optimizing the deposition parameters such as the duty cycle. The suitable process not only

Table 4
Fitted parameters for the TiC coatings as function of duty cycle in 0.05 M NaCl and 0.5 M H_2SO_4 derived from the equivalent circuit.

Solution	Duty cycle (%)	R_s ($\Omega\,cm^2$)	R_p ($k\Omega\,cm^2$)	CPE_{coat} ($\mu F\,cm^{-2}$)	n_c	R_{ct} ($k\Omega\,cm^2$)	CPE_{dl} ($\mu F\,cm^{-2}$)
0.05 M NaCl							
Bare steel		47	4287			1.8	5.1
	33	81	7945	12.87	0.89	2.9	3.62
TiC coating	40	94	11,967	10.56	0.91	4.1	2.11
	50	112	16,836	9.67	0.93	6.8	1.42
0.5 M H_2SO_4							
Bare steel		21	167			0.4	21.21
	33	35	1987	63	0.87	1.2	14.23
TiC coating	40	41	2789	182	0.92	2.6	12.16
	50	38	998	143	0.89	0.8	15.72

gives rise to a smooth surface morphology and fine grains, but also leads to enhanced electrochemical properties.

4. Conclusion

TiC coatings are deposited on hot-work steel (H_{11}) by plasma-assisted chemical vapor deposition using duty cycles of 33%, 40%, and 50%. Optimization of the deposition parameters such as duty cycles allows fine-tuning of the coating homogeneity, density, structure, and corrosion resistance in aggressive media such as NaCl and H_2SO_4 solutions. If the formation of pores is not covered up, firstly substrate corrosion and then coating delamination can occur. The EIS and potentiodynamic test results show that the electrochemical impedance of the TiC coatings is considerably higher than that of the bare steel in both solutions. The proper duty cycle in the PACVD process not only yields a smooth and fine-grained morphology, but also improves the electrochemical properties.

Acknowledgements

The authors would like to express their thanks to Iranian Nanotechnology Initiative Council. The work was financially supported by Hong Kong Research Grants Council (RGC) General Research Funds (GRF) No. CityU 112510 and City University of Hong Kong Applied Research Grant 9667038.

References

[1] L.R. Katipelli, A. Agarwal, N.B. Dahotre, Laser surface engineered TiC coating on 6061 Al alloy: microstructure and wear, Appl. Surf. Sci. 153 (2000) 65–78.
[2] A. Kumar, H.L. Chan, J.S. Kapat, Deposition an characterization of titanium carbide coatings using laser ablation method, Appl. Surf. Sci. 127 (1998) 549–552.
[3] A. Mani, P. Aubert, F. Mercier, H. Khodja, C. Berthier, P. Houdy, Effects of residual stress on the mechanical and structural properties of TiC thin films grown by RF sputtering, Surf. Coat. Technol. 194 (2005) 190–195.
[4] A.C. Fernandes, P. Carvalho, F. Vaz, S. Lanceros-Méndez, A.V. Machado, N.M.G. Parreira, J.F. Pierson, N. Martin, Property change in multifunctional TiC_xO_y thin films: effect of the O/Ti ratio, Thin Solid Films 515 (2006) 866–871.
[5] A. Leonhardt, K. Bartsch, I. Endler, Preparation and characterization of hard mono- and multilayer plasma assisted chemically vapour deposited coatings, Surf. Coat. Technol. 76–77 (1995) 225–230.
[6] S. Inoue, Y. Wada, K. Koterazawa, Deposition of TiC films by dual source dc magnetron sputtering, Vacuum 59 (2000) 735–741.
[7] I. Dahan, A. Admon, N. Frage, J. Sariel, M.P. Dariel, J.J. Moore, The development of a functionally graded TiC–Ti multilayer hard coating, Surf. Coat. Technol. 137 (2001) 111.
[8] B.D. Cullity, Elements of X-ray Diffraction, second ed., Addison Wesley, 1978.
[9] A. Niederhofer, T. Bolom, P. Nesladek, K. Moto, Ch. Eggs, D.S. Patil, S. Veprek, The role of percolation threshold for the control of the hardness and thermal stability of super- and ultrahard nanocomposites, Surf. Coat. Technol. 183 (2001) 146–147.
[10] M. Sakurai, T. Toihara, M. Wang, W. Kurosaka, S. Miyake, Surface morphology and mechanical properties of nanoscale TiAlN/SiNx multilayer coating deposited by reactive magnetron sputtering, Surf. Coat. Technol. 203 (2008) 171–179.
[11] K.N. Andersen, E.J. Bienk, Deposition, microstructure and mechanical and tribological properties of magnetron sputtered TiN/TiAlN multilayers, Surf. Coat. Technol. 219 (2000) 123.
[12] P.W. Shum, Z.F. Zhou, K.Y. Li, Optimisation of carbon implantation pretreatments on the adhesion strength of amorphous carbon coatings on AISI 440 C steel substrates, Surf. Coat. Technol. 166 (2003) 213–220.
[13] P.W. Shum, K.Y. Li, Z.F. Zhou, Y.G. Shen, Structural and mechanical properties of titanium–aluminium–nitride films deposited by reactive close-field unbalanced magnetron sputtering, Surf. Coat. Technol. 185 (2–3) (2004) 245–253.
[14] L.C. Fernandez-Torres, S.S. Perry, S.V. Didziulis, P.P. Frantz, The interaction of ammonia with transition metal carbide surfaces, Surf. Sci. 511 (2002) 121–132.
[15] D.A. Jones, Principles and Prevention of Corrosion, first ed., Macmillan, New York, 1992, p. 147.
[16] A.K. Singh, M.A. Quraishi, Effect of cafazolin on the corrosion of mild steel in HCl solution, Corros. Sci. 52 (2010) 152–160.
[17] M. Lebrini, M. Lagrenée, H. Vezin, M. Traisnel, F. Bentiss, Experimental and theoretical study for corrosion inhibition of mild steel in normal hydrochloric acid solution by some new macrocyclic polyether compounds, Corros. Sci. 49 (2007) 2254–2269.
[18] A. Zeng, E. Liu, I.F. Annergren, S.N. Tan, S. Zhang, P. Hing, J. Gao, EIS capacitance diagnosis of nanoporosity effect on the corrosion protection of DLC films, Diamond Relat. Mater. 11 (2002) 160.
[19] S.H. Ahn, J.H. Lee, H.G. Kim, J.G. Kim, Study on the quantitative determination of through-coating porosity in PVD-grown coatings, Appl. Surf. Sci. 233 (2004) 105.
[20] G.P. Bierwagen, L. He, J. Li, L. Ellingson, D.E. Tallman, Studies of a new accelerated evaluation method for coating corrosion resistance—thermal cycling testing, Prog. Org. Coat. 39 (2001) 67.
[21] E. Angelini, R. d'Agostino, F. Fracassi, S. Grassini, F. Rosalbino, Surface analysis of PECVD organosilicon films for corrosion protection of steel substrates, Surf. Interface Anal. 34 (2002) 155–159.
[22] X.L. Cheng, S.G. Roscoe, Corrosion behavior of titanium in the presence of calcium phosphate and serum proteins, Biomaterials 26 (2005) 7350.